



A 3D cross-linked graphene-based honeycomb carbon composite with excellent confinement effect of organic cathode material for lithium-ion batteries

Dong Sui^{a, b}, Lingqun Xu^a, Hongtao Zhang^a, Zhenhe Sun^a, Bin Kan^a, Yanfeng Ma^a, Yongsheng Chen^{a, *}

^a The Centre of Nanoscale Science and Technology and Key Laboratory of Functional Polymer Materials, State Key Laboratory and Institute of Elemento-Organic Chemistry, College of Chemistry, Nankai University, Tianjin, 300071, China

^b Key Laboratory of Function-Oriented Porous Materials, College of Chemistry and Chemical Engineering, Luoyang Normal University, Luoyang, 471934, China

ARTICLE INFO

Article history:

Received 14 September 2019

Received in revised form

24 October 2019

Accepted 31 October 2019

Available online 3 November 2019

ABSTRACT

Organic cathode materials are drawing increasing attention in lithium-ion battery for their abundance, environmental friendliness, high specific capacity, low cost, and flexibility. But their application has been hindered by poor electrochemical performance because of inherent low conductivity and high solubility in the polar organic electrolyte. Herein, an organic-inorganic composite by impregnating electrochemically active 4,8-dihydrobenzo [1,2-b:4,5-b'] dithiophene-4,8-dione (BDT) into the pores of 3D cross-linked graphene-based honeycomb carbon (3DGraphene) has been prepared, which not only offers a highly conductive framework with plenty of interconnected pores from the 3D graphene network, but also simultaneously overcomes the two typical drawbacks of organic cathode materials. The excellent confinement effect of the nanopores and the strong π - π interaction between BDT and 3DGraphene largely avoid the dissolution of BDT in the electrolyte. Therefore, the obtained BDT/3DGraphene composite shows a much improved good rate capability (more than 100 mAh g⁻¹ at 4.0C vs less than 50 mAh g⁻¹ for BDT) and cycling stability (about 80% capacity retention at 0.5C while only ~14% for BDT for 200 cycles), as well as high reversible specific capacity (over 210 mAh g⁻¹).

© 2019 Elsevier Ltd. All rights reserved.

1. Introduction

Electrochemical energy storage devices, especially lithium-ion batteries (LIBs), are indispensable for the portable electronics, electric vehicles, and emerging large-scale energy storage systems, not to mention that for the utilization of renewable and clean but intermittent power sources like solar and wind [1–3]. However, the state-of-the-art LIBs based on non-renewable insertion-mechanism inorganic electrode materials are reaching the limit of their energy density for the widely used transition metal-based cathodes [4–6]. Furthermore, the process of extraction and synthesis of these inorganic oxide compounds is often energy intensive and also creates large amounts of toxic materials and heavy metal waste [7–9]. Therefore, organic electrode materials have been intensively

investigated these days as cathodes for LIBs because of their easy processability, lightweight, redox stability, structural diversity, resource recyclability, infinite availability from environmentally friendly materials, and potential flexibility and low cost [10–14]. In particular, some quinone-based compounds with tunable and diverse structure, two-electron redox behavior, high theoretical specific capacity, and electrochemical reversibility are among the most promising organic electrode materials to replace the traditional inorganic cathodes for the next generation of advanced LIBs [15–20]. However, the practical applications of such organic cathodes have been impeded by mainly two factors including their high solubility in the aprotic electrolyte (especially small organic molecules) and intrinsically low electronic conductivity. These drawbacks are leading to serious shuttle effect and inefficient use of active materials, rapid capacity decrease and inferior rate capability.

Generally, to overcome the troublesome dissolution of small organic compounds in electrolyte, several effective methods have

* Corresponding author.

E-mail address: yschen99@nankai.edu.cn (Y. Chen).

been applied to enhance the utilization of the active materials during the charge/discharge process, including formation of polymer [16,21–23], oligomer or organic salts [13,19,20,24], anchoring onto carbon nanotubes [25], and optimization of the electrolyte by additive [26] or replacing traditional liquid electrolyte with gel-state electrolyte [27]. But these approaches still have some disadvantages concerning poor electronic conductivity and low anchoring efficiency. Recently, carbon-based nanostructured materials like carbon nanotubes and mesoporous carbon are applied to load organic materials and exhibit superior electrochemical performance [23,28,29]. However, the dissolution problem of organic cathodes still exists due to the miserable confinement of the substrate and the weak interaction between them. Therefore, we need to design an ideal host for organic cathode, which should have the following merits: 1) 3D porous structure with high conductivity; 2) high specific surface area and large pore volume; 3) strong interaction with organic molecule.

Graphene, a single-layer sheet composed of sp^2 hybridized carbon, has extraordinary properties of large theoretical specific surface area (SSA), high electronic conductivity and high chemical stability and shows promising applications in energy storage materials [30–33]. Several groups have used graphene as the conductive additives or loading substrates for organic cathode materials [18,34,35]. However, graphene, if used directly, is still not an effective matrix to confine soluble small organic molecules because of severe aggregation and lack of nanostructured pores, so the “shuttle” problem still exists during charge/discharge process. Therefore, it is highly demanded to design a novel structure to load higher content of active materials, which should not only ensure excellent electronic conductivity but also confine the soluble organic materials in the composites effectively.

Our group have developed a three-dimensional graphene-based honeycomb type carbon (3DGraphene) with high SSA and large pore volume and successfully applied in supercapacitors, Li–S, and lithium-ion capacitors [36–38]. This 3DGraphene is expected to be an excellent host for organic cathode materials due to the following reasons. Above the strong π - π interaction between the graphene sheets in 3DGraphene and quinone-based organic cathode materials, its hierarchical honeycomb pore structure can not only load more organic cathode materials but also depress the solubility of organic cathode in the polar aprotic electrolyte due to its strong confinement effect, thus improving cycling stability. Furthermore, the superior electronic conductivity and plenty of interconnected pores of 3DGraphene can facilitate electron and ion transport, so that the rate capability of the composite could also be enhanced. Note that electrochemically active 4,8-dihydrobenzo [1,2-*b*:4,5-*b'*] dithiophene-4,8-dione (BDT) has high reversible specific capacity and contains large ring conjugate aromatic structure which can form strong π - π interaction with graphene-based materials. Thus, in this work, a BDT/3DGraphene composite was fabricated by loading BDT into the nanopores of 3DGraphene with a simple impregnation method, and the multiple effects from 3DGraphene on the lithium ion storage properties of BDT were examined. The electrochemical studies of the as-prepared BDT/3DGraphene composite demonstrate that the problems of poor electronic conductivity and solubility in electrolyte associated with small organic cathode materials such as BDT in this case can be simultaneously overcome. Compared with the case using BDT directly, BDT/3DGraphene composite shows much improved rate capability of 100 mAh/g at 4C (less than 50 mAh g^{-1} for BDT) and better cycling stability with over four times higher than that of using BDT. All these results are ascribed to the effective restriction of the nanostructured honeycomb pores and the high electrical conductivity of graphene-based carbon framework in 3DGraphene.

2. Experimental

2.1. Materials synthesis

2.1.1. Synthesis of 3D cross-linked graphene-based honeycomb carbon

The synthesis of the 3D cross-linked graphene-based honeycomb carbon material has been reported in our previous work [36]. In a typical synthesis of 3DGraphene, 0.35 g graphite oxide was homogeneously dispersed in 70 ml water by ultrasonication to form a stable aqueous dispersion of graphene oxide (GO), then 2.34 g phenol (P) and 3.36 g formaldehyde (F) (35 wt %) were added into the GO solution. After stirring for 30 min, the homogeneous dispersion was transferred to a sealed 100 ml Teflon-lined autoclave, heated up to 180 °C and maintained at 180 °C for 12 h. The resulting solid product was then washed with distilled water and finally dried in vacuum at 120 °C for 24 h. The obtained intermediate product was mixed with 4 times weight of KOH, and heated at 5 °C min^{-1} to 900 °C for 1 h under Ar. After cooling down to room temperature, the product was thoroughly washed with 0.1 M HCl to remove any inorganic salts, then washed with distilled water until the pH value reached 7, and finally the 3D cross-linked graphene-based honeycomb carbon with plenty of interconnected pores was obtained after being dried in vacuum at 120 °C for 24 h.

2.1.2. Synthesis of 4,8-dihydrobenzo[1,2-*b*:4,5-*b'*] dithiophene-4,8-dione/3D cross-linked graphene-based honeycomb carbon (BDT/3DGraphene) composite

The BDT/3DGraphene composite was prepared by a simple impregnation method. In a typical synthesis process, 300 mg BDT was firstly dissolved in N-Methyl pyrrolidone (NMP) to obtain BDT/NMP solution (10 wt%), then 200 mg 3DGraphene was added to the solution, and the mixture was stirred at room temperature for 30 min. After that, NMP was removed under vacuum. The obtained powder was heated at 265 °C for 3 h in a sealed vessel under Ar and finally the BDT/3DGraphene composite with a mass ratio of 1.5:1 was collected. BDT/3DGraphene composites with mass ratios of 1:1 and 2:1 were also prepared with similar method.

2.2. Characterization

Scanning Electron Microscopy (SEM) and Energy Dispersive X-ray Spectroscopy (EDS) images were obtained using LEO 1530 VP field emission scanning electron microscope with an acceleration voltage of 10 kV. Powder X-ray diffraction (XRD) patterns were collected on a Rigaku D/Max-2500 diffractometer with Cu KR radiation. The Raman spectra were examined with a LabRAM HR Raman spectrometer using laser excitation at 514.5 nm. Thermogravimetric analysis (TGA) was carried out for thermal stability measurements from room temperature to 600 °C at a heating rate of 10 °C min^{-1} in N_2 using a NETZSCH STA-409PC instrument. The nitrogen adsorption/desorption analysis was conducted at 77 K on a Micromeritics ASAP 2020 apparatus. The specific surface area was calculated by the BET (Brunauer-Emmett-Teller) method based on adsorption data in the relative pressure (P/P_0) range of 0.05–0.3. The pore size distribution was analyzed using a NL-DFT (Nonlocal Density Functional Theory) method with a slit pore model from the nitrogen adsorption data.

2.3. Cell fabrication and electrochemical characterization

Electrochemical measurements of the samples were carried out by assembling coin-type cells in a glove box filled with argon. To prepare the working electrodes, BDT/3DGraphene composite and polytetrafluoroethylene with a mass ratio of 9:1 were directly

mixed, and rolled into thin sheets, which were then punched into 1 cm diameter electrodes and hot pressed onto carbon-coated aluminum foil with a mass loading of ~ 4 mg. After heating at 90°C for 3 h under vacuum, the coin-type cells were assembled in an argon-filled glovebox with lithium metal foil as the counter/reference electrode. The electrolyte used was lithium bis-(trifluoromethanesulfonyl)imide (1 M) in 1:1 (v/v) 1,2-dimethoxy ethane and 1,3-DOL, containing 2 wt % LiNO_3 . The charge/discharge measurements were conducted using a battery test system (LAND CT2001A model, Wuhan LAND Electronics, Ltd.) at an operational voltage window from 1.5 to 3.5 V at room temperature and the specific capacity was calculated based on the mass of BDT. Cyclic voltammetry (CV) and Electrochemical impedance spectral (EIS) measurements were performed using an Autolab system (Metrohm). CV tests were carried out at a scan rate of 0.1 mV s^{-1} with a potential range of 1.5–3.5 V. EIS measurements were carried out at AC amplitude of 5 mV, and the frequency range was from 100 mHz to 100 KHz. As a control, the BDT electrode composed of 54 wt% BDT, 36 wt% Super P and 10 wt% PTFE were also prepared, and its electrochemical performance was compared with that of BDT/3DGraphene.

3. Results and discussion

The BDT/3DGraphene composite was facilely prepared by impregnating the electrochemically active BDT into the pores of highly conductive 3D graphene-based honeycomb carbon following the previous procedure before [36,38], as demonstrated in Fig. 1. Firstly, phenol and formaldehyde were in-situ polymerized to form phenolic resin on the surface of GO during the hydrothermal process. Then the intermediate product was chemically activated by KOH at 900°C and 3DGraphene with high electrical conductivity and hierarchical structure was obtained. Finally, the BDT was loaded into the interconnected nanopores to get the BDT/3DGraphene composite using a simple impregnation method.

The morphology and microstructure of 3DGraphene and BDT/3DGraphene composites with different content of BDT were characterized by SEM (Fig. 2 and Fig. S1). As shown in Fig. 2a, the graphene modified phenolic resin was converted into three dimensional cross-linked honeycomb carbon material with fuzzy surface and abundant pores after chemical activation at high temperature, endowing the 3DGraphene with large SSA and pore volume besides a high conductivity, as has been demonstrated before [36,39]. Materials of such typical porous structure are proved to be a perfect matrix to load non-conductive materials such as S and organic cathodes [26,38]. As we can see in Fig. 2b, c, and 2d, the overall structure of 3DGraphene is well-kept after impregnation of BDT, but their surfaces become smoother with increase of the mass ratio of BDT and 3DGraphene, demonstrating that BDT was successfully loaded into the pores of 3DGraphene. Especially for the sample with a mass ratio of 2:1, the pores in it completely disappear, and the excess BDT was presented on the external surface of

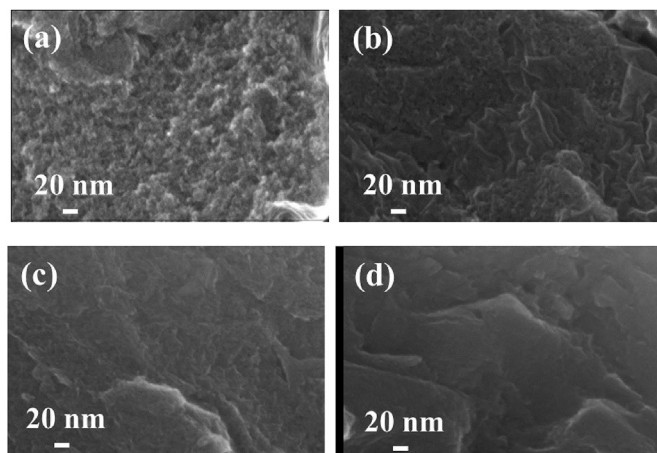


Fig. 2. SEM images of (a) 3DGraphene, and BDT/3DGraphene composites with mass ratios of (b)1:1, (c)1.5:1, (d)2:1.

3DGraphene, from which we suppose such high quantity of BDT is out of the loading capacity of the pores of 3DGraphene. Moreover, the BDT existing on the outside of 3DGraphene is detrimental to its electrochemical properties because of the high solubility of BDT and its lithiation state in polar organic electrolytes.

The porosity properties of 3DGraphene and BDT/3DGraphene composites were investigated by nitrogen adsorption/desorption experiments, as displayed in Fig. 3 and Table S1. According to the nitrogen adsorption data, 3DGraphene shows both high SSA ($2803.1\text{ cm}^2\text{ g}^{-1}$) and large pore volume ($1.79\text{ cm}^3\text{ g}^{-1}$) with the pore size distribution of 1–10 nm, which can ensure a high loading content of BDT. But after the impregnation of BDT, the SSA sharply decreases to $464.9\text{ cm}^2\text{ g}^{-1}$ for BDT/3DGraphene (1:1) and further to $93.3\text{ cm}^2\text{ g}^{-1}$ for BDT/3DGraphene (1.5:1), while the pore volume drops to 0.45 and $0.13\text{ cm}^3\text{ g}^{-1}$, respectively. What's more, the micropores of 1–2 nm are gradually diminished, and the mesopores with the size of 2–10 nm are largely depressed. There is no doubt that BDT was successfully loaded into the pores of 3DGraphene through the simple impregnation method. However, the SSA is only $22.1\text{ cm}^2\text{ g}^{-1}$, and the pore volume can be neglected for the BDT/3DGraphene (2:1) composite, suggesting BDT was over-loaded. Combining the porosity properties analysis and SEM images of these composites, it can be concluded that BDT/3DGraphene (1:1) has insufficient loading of BDT while BDT/3DGraphene (2:1) is too much. Therefore, we choose BDT/3DGraphene (1.5:1) for further study and compare its electrochemical performance with that of BDT.

As discussed above, BDT is evenly dispersed in the pores of 3DGraphene for the optimal mass ratio of 1.5:1, which can be further reflected by other characterizations discussed below. As shown in Fig. 4a of EDS measurements, the element oxygen and sulfur of BDT are highly homogeneous distributed in the whole BDT/3DGraphene composite. XRD was used to characterize the crystal structure of 3DGraphene, BDT, and BDT/3DGraphene composite. Clearly, pure BDT (JCPDS no. 05-005-3387) exists in a good crystalline state with sharp diffraction patterns, which can be indexed to a monoclinic structure (space group: $P2_1/n$, lattice constants: $a = 5.6402\text{ \AA}$, $b = 5.7745\text{ \AA}$, $c = 13.6223\text{ \AA}$), in a good match with other report and simulation [40,41]. 3DGraphene shows an amorphous state and only a very weak and extremely suppressed broad peak between 15° and 30° because of chemical activation. After filling BDT into the pores of 3DGraphene, its typical diffraction peaks vanished completely while a strong broad peak at about 25° presents, demonstrating that the BDT exists in a highly

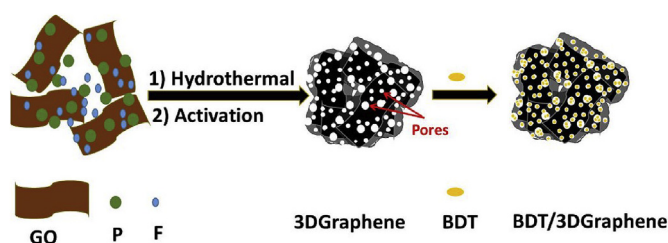


Fig. 1. Schematic of the fabrication of the BDT/3DGraphene composite. (A colour version of this figure can be viewed online.)

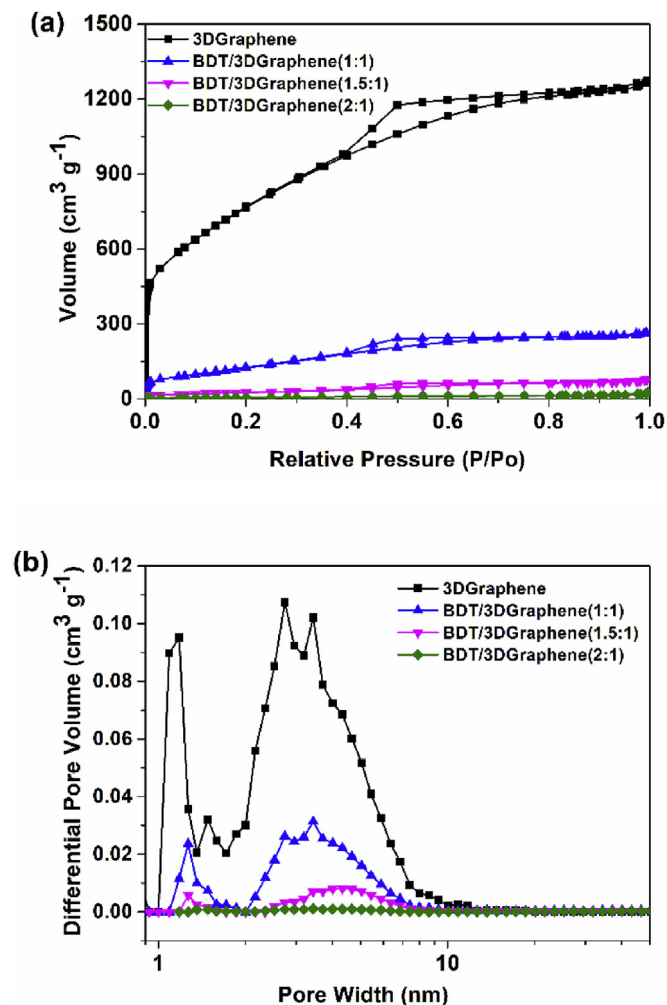


Fig. 3. (a) The nitrogen adsorption/desorption isotherms and (b) pore-size distributions of 3DGraphene and BDT/3DGraphene with various mass ratios. (A colour version of this figure can be viewed online.)

dispersed amorphous state which could enhance the utilization of the active material in the electrochemical reactions. The Raman spectra of 3DGraphene, BDT, and BDT/3DGraphene composite are displayed in Fig. 4c and Fig. S2. For 3DGraphene, there are two broad peaks at $\sim 1350\text{ cm}^{-1}$ (D band) and $\sim 1580\text{ cm}^{-1}$ (G band), which can be ascribed to the defects and sp^2 carbon networks, respectively. BDT shows typical peaks in the range of $400\text{--}1800\text{ cm}^{-1}$, but only a small weak peaks exists at 1431 and 1647 cm^{-1} in the BDT/3DGraphene composite, indicating that all the BDT is loaded in the pores of 3DGraphene in a highly amorphous state without long-range ordering, which is well consistent with the conclusion from XRD patterns. TGA was used to determine the content of BDT, amounting to 59.5 wt% of the BDT/3DGraphene composite, as shown in Fig. 4d. It should be noted that the BDT loaded in the 3DGraphene is more stable than in the pure state because of the strong π - π interaction and the effective confinement of the pores of 3DGraphene, which is supposed to decrease the solubility and diffusion of BDT and its lithiated state in the organic electrolyte.

Based on the above analysis, 3DGraphene has plenty of interconnected pores with high SSA and large pore volume, making it a perfect matrix to load BDT for lithium ion battery. More importantly, the strong π - π interaction between BDT and 3DGraphene further enhances the confinement of the pores. By impregnating

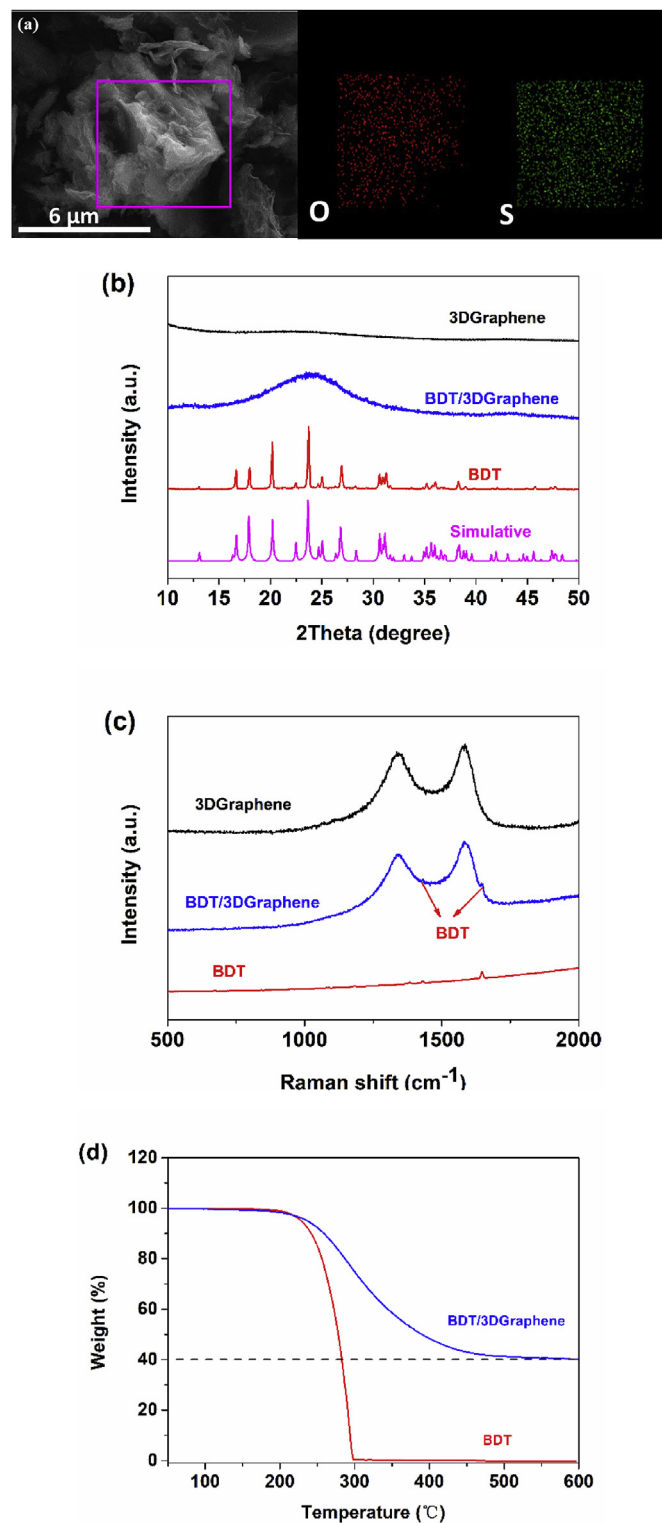


Fig. 4. (a) EDS elemental mappings of BDT/3DGraphene composite; (b) XRD patterns and (c) Raman spectra of the 3DGraphene, BDT powder and BDT/3DGraphene composite; (d) TGA curves of BDT and the prepared BDT/3DGraphene composite. (A colour version of this figure can be viewed online.)

BDT into the pores of 3D cross-linked graphene-based porous carbon, the problems of BDT associated with high solubility in organic electrolytes can be solved. 3DGraphene with high inherent electrical conductivity forms good three-dimensional conductive

network and can help to overcome the non-conductivity of BDT. Therefore, BDT/3DGraphene could be expected to have good electrochemical performance because of the synergetic effect of the two components.

The electrochemical properties of the BDT/3DGraphene composite were evaluated using half cells. From the CV curves of BDT/3DGraphene at 0.1 mV s^{-1} (Fig. 5a), we can see two main redox peaks at 2.49 V and 2.67 V corresponding to the reduction (lithiation) and oxidation (de-lithization) process of the carbonyl groups (inset of Fig. 5a). As shown in the galvanostatic charge/discharge profiles for the first three cycles at 0.1C ($1\text{C} = 243 \text{ mA g}^{-1}$) in Fig. 5b, BDT/3DGraphene displays an initial discharge capacity of $\sim 208 \text{ mAh g}^{-1}$, which slightly increases to $\sim 215 \text{ mAh g}^{-1}$ (amounting to 88.4% of the theoretical capacity of BDT and higher than other report [18]) in the second cycle because of better contact between active material and electrolyte and easy lithium ion transport. What's more, consistent with the redox peaks of CV curves, it demonstrates an apparent flat charge/discharge plateau of around 2.5 V. It should also be noted that the distance between the two redox peaks or charge/discharge plateau is minimal and the lithiation/de-lithiation process is highly reversible, indicating that 3DGraphene with high conductivity and abundant interconnected pores is favorable to electron and lithium ion transportation for the BDT/3DGraphene composite.

The rate capability of the BDT/3DGraphene composite and BDT was investigated at different rates, as shown in Fig. 5c. Compared with the directly used BDT, the 3DGraphene-based composite demonstrates a much better rate performance, especially at high rates. Specifically, BDT/3DGraphene delivers 205 and 160 mAh g^{-1} at 0.2 and 0.5C, respectively, which is over 60 mAh g^{-1} higher than that of BDT. Even at the high rate of 4C, BDT/3DGraphene still maintains a specific capacity of $\sim 100 \text{ mAh g}^{-1}$, whereas the discharge capacity of BDT is less than 40 mAh g^{-1} , demonstrating an excellent rate performance for the composite. The improved rate capability of the composite is ascribed to the uniformly dispersed amorphous state BDT with high electrochemical activity, high electronic conductivity of 3DGraphene to facilitate electron transport, and abundant interconnected pores of the matrix to help lithium ion transport and also shorten the ion diffusion distance.

Fig. 5d present the cycling performance of the BDT/3DGraphene composite and BDT at 0.5C. Not surprisingly, BDT loaded in the pores of 3DGraphene shows higher capacity and much better cycling stability than that of BDT over the whole 200 cycles. BDT/3DGraphene delivers an initial discharge capacity of 178 mAh g^{-1} and still maintains 142 mAh g^{-1} after 200 cycles with capacity retention of about 80% and stable Coulombic efficiency (CE) of $\sim 100\%$. However, BDT exhibits inferior initial capacity (only $\sim 140 \text{ mAh g}^{-1}$) at 0.5C compared with BDT/3DGraphene, indicating lousy utilization of the active material, which is properly due to the poor contact between BDT and conductive additive. Furthermore, the discharge capacity decays rapidly, and only $\sim 20 \text{ mAh g}^{-1}$ ($\sim 14\%$ capacity retention) remains after 200 cycles with a fluctuant CE over 100% through the 200 cycles resulting from the dissolution of BDT in the electrolyte. As designed, these results illustrate that the 3DGraphene matrix could effectively improve the cycling performance of BDT, which is attributed to the confinement of the abundant 3D interconnected nanopores and the strong π - π interaction between BDT and 3DGraphene. This could be further confirmed by the results that no clear defect was observed for the integrated and uniform morphologies of BDT/3DGraphene electrode after 200 cycles (see Fig. S3). The BDT/3DGraphene also shows superiority electrochemical performances over the state-of-the-art organic cathode composites with carbon-based substrates in terms of cycling stability and rate capability, as can be seen in Table 1.

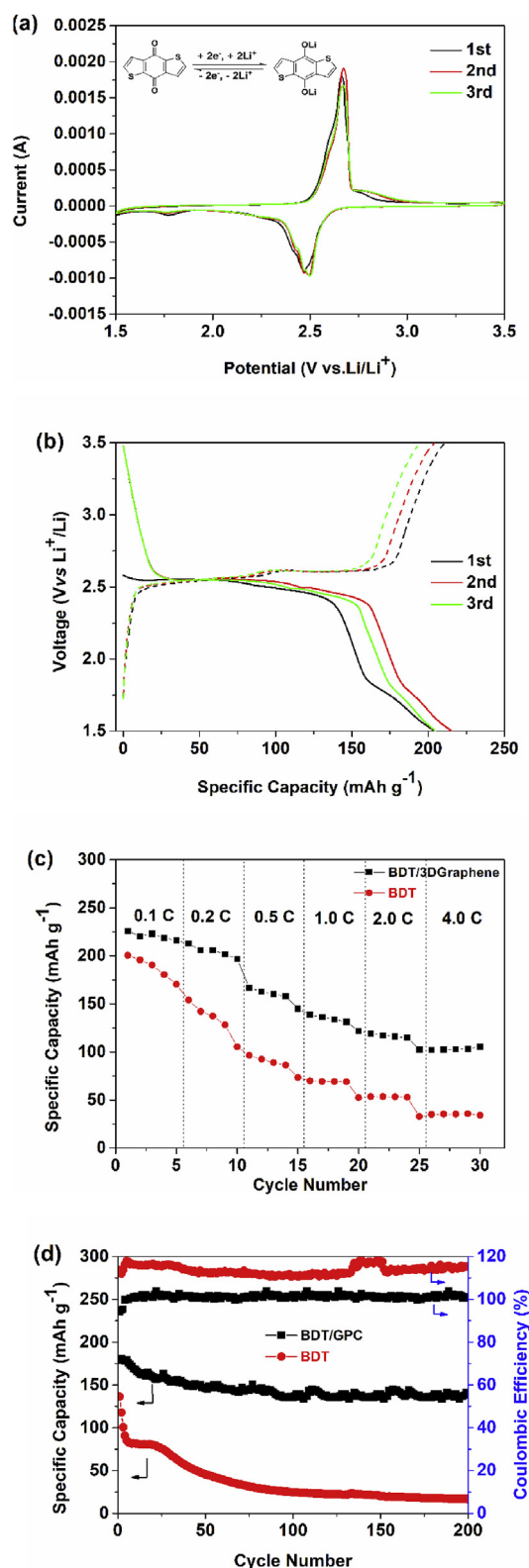


Fig. 5. (a) CV curves of BDT/3DGraphene at a sweep rate of 0.1 mV s^{-1} for the first three cycles (Inset: the proposed electrochemical redox mechanism of BDT); (b) Discharge-charge curves at 0.1C of BDT/3DGraphene composite for the first, second, and third cycles; (c) The rate capability of BDT/3DGraphene composite and BDT; (d) The cycling performance and the corresponding Coulombic efficiency of BDT/3DGraphene and BDT at 0.5C. (A colour version of this figure can be viewed online.)

Table 1
The electrochemical performances of recently reported organic cathode composites.

Sample	Voltage range (V)	Cycles/capacity retention	Rate capability (mAh g ⁻¹)/capacity retention	Reference
BDT/3DGraphene	1.5–3.5	200/80% @ 0.5C	100/46.5% @ 4C	This work
PI/FLEG	1.5–3.5	200/80% @ 0.5C	38/21.5% @ 5C	[42]
DNTCB-GO	1.5–4.5	50/85% @ 0.1C	60/42.8% @ 4C	[43]
AQ/CMK-3	2.0–2.8	100/84.9% @ 0.2C	146/69.2% @ 2C	[26]
MC/AQ	1.5–3.5	50/38.3% @ 1.2C	96/43.2% @ 2.3C	[44]
H ₂ bhnq/CMK-3	1.5–3.5	50/65.6% @ 0.1C	150/48.6% @ 5C	[29]
BDTD/graphene	1.5–3.5	100/65% @ 0.1C	~80/38.5% @ 5C	[18]

In order to further understand their electrochemical performance, EIS measurements were conducted on the BDT/3DGraphene composite and BDT electrodes before and after 200 cycles at 0.5C. As shown in Fig. 6, both the samples exhibit higher impedances after 200 cycles and all of the profiles show a semicircle in the high-middle frequency region and an inclined line in the low-frequency region. The semicircle can be assigned to the combination of the charge-transfer resistance (R_{ct}) at the electrode surface and the double-layer capacitance (CPE) between the electrolyte and the cathode while the inclined line is attributed to Warburg impedance (W_z) of the Li⁺ transport in the electrode [29,38]. The simulated values of EIS by using the equivalent circuit model (inset of Fig. 6) are summarized in Table S2. It can be seen that all the samples show comparable ohmic resistance (R_s) which is related to the electrolyte and contact resistances and BDT/3DGraphene samples demonstrate lower W_z . Apparently, it could be concluded that the resistance of BDT associated with charge transfer is much higher than that of BDT/3DGraphene at the same cycle from the diameter of the semicircle [45], demonstrating that the conductivity can be significantly increased after the uniform impregnation of BDT into the nanopores of 3DGraphene due to good contact and high conductivity of the graphene-based porous carbon matrix.

All the above results indicate that 3DGraphene, with high conductivity and unique microstructure, can effectively enhance the electrochemical performances of BDT because of the following reasons. First of all, BDT filled in the nanopores of 3DGraphene is highly dispersed with an amorphous state and therefore provides more active sites for the electrochemical reaction and enables the full utilization of active materials. Secondly, the dissolution of BDT in the electrolyte can be effectively restricted because of the confinement effect of the abundant interconnected nanopores of 3DGraphene and the strong π - π interaction between 3DGraphene and BDT. Overall, the highly conductive graphene-based porous carbon framework facilitates both the electron and lithium ion

transportation through the whole electrode. Therefore, by impregnation of BDT into the pores 3DGraphene, the composite shows much better electrochemical performance.

4. Conclusions

BDT/3DGraphene composite has been prepared by employing a facile impregnation of the electrochemically active BDT into the nanopores of 3D graphene-based honeycomb carbon matrix. All the characterizations have shown that BDT, which is in an amorphous and highly dispersed state, was successfully loaded into the interconnected pores of 3DGraphene. The BDT/3DGraphene composite demonstrates excellent electrochemical results with a reversible capacity of over 210 mAh g⁻¹ at 0.1C, good rate capability (100 mAh g⁻¹ at 4.0C vs 40 mAh g⁻¹ for BDT), and stable cycling of 80% capacity retention at 0.5C (only ~14% for BDT) for 200 cycles. The enhanced performance of BDT/3DGraphene can be attributed to the introduction of 3DGraphene as the matrix, which simultaneously increases the conductivity and inhibits the dissolution of BDT. Moreover, the method used in this work could be applied to other organic cathode materials which have the same problems of inherent low conductivity and high solubility in an organic electrolyte.

Declaration of competing interest

The authors declare that they have no known competing financial interests or personal relationships that could have appeared to influence the work reported in this paper.

Acknowledgments

The authors gratefully acknowledge the financial support from Ministry of Science and Technology of China (#2016YFA0200200), the National Natural Science Foundation of China (#21421001,51633002,51472124), Tianjin city (16ZXCLGX00100) and 111 Project.

Appendix A. Supplementary data

Supplementary data to this article can be found online at <https://doi.org/10.1016/j.carbon.2019.10.106>.

References

- [1] M. Armand, J.M. Tarascon, Building better batteries, *Nature* 451 (7179) (2008) 652–657.
- [2] N. Wu, X. Qiao, J. Shen, G. Liu, T. Sun, H. Wu, et al., Anatase inverse opal TiO_{2-x}@N-doped C induced the dominant pseudocapacitive effect for durable and fast lithium/sodium storage, *Electrochim. Acta* 299 (2019) 540–548.
- [3] G. Liu, J. Cui, R. Luo, Y. Liu, X. Huang, N. Wu, et al., 2D MoS₂ grown on biomass-based hollow carbon fibers for energy storage, *Appl. Surf. Sci.* 469 (2019) 854–863.
- [4] M.S. Whittingham, Lithium batteries and cathode materials, *Chem. Rev.* 104 (10) (2004) 4271–4301.
- [5] J.B. Goodenough, Y. Kim, Challenges for rechargeable Li batteries, *Chem.*

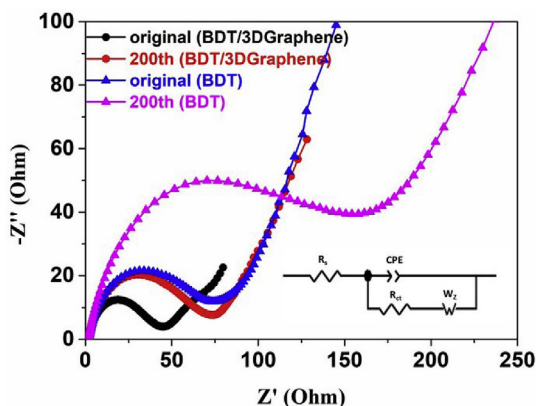


Fig. 6. The electrochemical impedance spectra of BDT/3DGraphene and BDT before and after 100th cycles. (A colour version of this figure can be viewed online.)

- Mater. 22 (3) (2010) 587–603.
- [6] G. Liu, M. Li, N. Wu, L. Cui, X. Huang, X. Liu, et al., Single-crystalline particles: an effective way to ameliorate the intragranular cracking, thermal stability, and capacity fading of the $\text{LiNi}_{0.6}\text{Co}_{0.2}\text{Mn}_{0.2}\text{O}_2$ electrodes, *J. Electrochem. Soc.* 165 (13) (2018) A3040–A3047.
- [7] T.B. Schon, B.T. McAllister, P.-F. Li, D.S. Seferos, The rise of organic electrode materials for energy storage, *Chem. Soc. Rev.* 45 (22) (2016) 6345–6404.
- [8] S. Muench, A. Wild, C. Friebe, B. Haeupler, T. Janoschka, U.S. Schubert, Polymer-based organic batteries, *Chem. Rev.* 116 (16) (2016) 9438–9484.
- [9] N. Wu, H. Wu, J.-K. Kim, X. Liu, Y. Zhang, Restoration of degraded nickel-rich cathode materials for long-life lithium-ion batteries, *ChemElectroChem* 5 (1) (2017) 78–83.
- [10] Y. Liang, Z. Tao, J. Chen, Organic electrode materials for rechargeable lithium batteries, *Adv. Energy Mater.* 2 (7) (2012) 742–769.
- [11] Z. Song, H. Zhou, Towards sustainable and versatile energy storage devices: an overview of organic electrode materials, *Energy Environ. Sci.* 6 (8) (2013) 2280–2301.
- [12] Z. Luo, L. Liu, Q. Zhao, F. Li, J. Chen, An insoluble benzoquinone-based organic cathode for use in rechargeable lithium-ion batteries, *Angew. Chem. Int. Ed.* 56 (41) (2017) 12561–12565.
- [13] Z. Song, Y. Qian, M.L. Gordin, D. Tang, T. Xu, M. Otani, et al., Polyanthraquinone as a reliable organic electrode for stable and fast lithium storage, *Angew. Chem. Int. Ed.* 54 (47) (2015) 13947–13951.
- [14] S. Lee, G. Kwon, K. Ku, K. Yoon, S.K. Jung, H.D. Lim, et al., Recent progress in organic electrodes for Li and Na rechargeable batteries, *Adv. Mater.* 30 (42) (2018), 1704682.
- [15] H.L. Peng, Q.C. Yu, S.P. Wang, J. Kim, A.E. Rowan, A.K. Nanjundan, et al., Molecular design strategies for electrochemical behavior of aromatic carbonyl compounds in organic and aqueous electrolytes, *Adv. Sci.* 6 (17) (2019), 1900431.
- [16] Y. Lu, X.S. Hou, L.C. Miao, L. Li, R.J. Shi, L.J. Liu, et al., Cyclohexanehexone with ultrahigh capacity as cathode materials for lithium-ion batteries, *Angew. Chem. Int. Ed.* 58 (21) (2019) 7020–7024.
- [17] B. Häupler, A. Wild, U.S. Schubert, Carbonyls: powerful organic materials for secondary batteries, *Adv. Energy Mater.* 5 (11) (2015), 1402034.
- [18] Y. Liang, P. Zhang, S. Yang, Z. Tao, J. Chen, Fused heteroaromatic organic compounds for high-power electrodes of rechargeable lithium batteries, *Adv. Energy Mater.* 3 (5) (2013) 600–605.
- [19] Z. Song, Y. Qian, X. Liu, T. Zhang, Y. Zhu, H. Yu, et al., A quinone-based oligomeric lithium salt for superior Li-organic batteries, *Energy Environ. Sci.* 7 (12) (2014) 4077–4086.
- [20] T. Nokami, T. Matsuo, Y. Inatomi, N. Hojo, T. Tsukagoshi, H. Yoshizawa, et al., Polymer-bound pyrene-4,5,9,10-tetraone for fast-charge and -discharge lithium-ion batteries with high capacity, *J. Am. Chem. Soc.* 134 (48) (2012) 19694–19700.
- [21] A.V. Mummyatov, A.F. Shestakov, N.N. Dremova, K.J. Stevenson, et al., New naphthalene-based polyimide as an environment-friendly organic cathode material for lithium batteries, *Energy Technol.* 7 (5) (2019), 1801016.
- [22] G. Wang, N. Chandrasekhar, B.P. Biswal, D. Becker, S. Paasch, E. Brunner, et al., A crystalline, 2D polyarylimide cathode for ultrastable and ultrafast Li storage, *Adv. Mater.* 31 (28) (2019), 1901478.
- [23] J.H. Zhao, T. Kang, Y.L. Chu, P. Chen, F. Jin, Y.B. Shen, et al., A polyimide cathode with superior stability and rate capability for lithium-ion batteries, *Nano Research* 12 (6) (2019) 1355–1360.
- [24] S. Wang, L. Wang, K. Zhang, Z. Zhu, Z. Tao, J. Chen, Organic $\text{Li}_4\text{C}_8\text{H}_{20}\text{O}_6$ nano-sheets for lithium-ion batteries, *Nano Lett.* 13 (9) (2013) 4404–4409.
- [25] G. Charrier, A. Desrués, C. Barchasz, J. Leroy, R. Cornut, B. Jusselme, et al., Covalently functionalized carbon nanotubes as stable cathode materials of lithium/organic batteries, *J. Mater. Chem.* 4 (39) (2016) 15036–15040.
- [26] K. Zhang, C. Guo, Q. Zhao, Z. Niu, J. Chen, High-performance organic lithium batteries with an ether-based electrolyte and 9,10-anthraquinone (AQ)/CMK-3 cathode, *Adv. Sci.* 2 (5) (2015), 1500018.
- [27] Z. Zhu, M. Hong, D. Guo, J. Shi, Z. Tao, J. Chen, All-solid-state lithium organic battery with composite polymer electrolyte and pillar[5]quinone cathode, *J. Am. Chem. Soc.* 136 (47) (2014) 16461–16464.
- [28] M. Lee, J. Hong, H. Kim, H.D. Lim, S.B. Cho, K. Kang, et al., Organic nanohybrids for fast and sustainable energy storage, *Adv. Mater.* 26 (16) (2014) 2558–2565.
- [29] H. Li, W. Duan, Q. Zhao, F. Cheng, J. Liang, J. Chen, 2,2'-Bis(3-hydroxy-1,4-naphthoquinone)/CMK-3 nanocomposite as cathode material for lithium-ion batteries, *Inorg. Chem. Front.* 1 (2) (2014) 193–199.
- [30] Y. Wang, Z.Q. Shi, Y. Huang, Y.F. Ma, C.Y. Wang, M.M. Chen, et al., Supercapacitor devices based on graphene materials, *J. Phys. Chem. C* 113 (30) (2009) 13103–13107.
- [31] Z.S. Wu, W.C. Ren, L. Xu, F. Li, H.M. Cheng, Doped graphene sheets as anode materials with superhigh rate and large capacity for lithium ion batteries, *ACS Nano* 5 (7) (2011) 5463–5471.
- [32] Y. Sun, Q. Wu, G. Shi, Graphene based new energy materials, *Energy Environ. Sci.* 4 (4) (2011) 1113–1132.
- [33] S. Han, D. Wu, S. Li, F. Zhang, X. Feng, Porous graphene materials for advanced electrochemical energy storage and conversion devices, *Adv. Mater.* 26 (6) (2014) 849–864.
- [34] H.L. Lyu, P.P. Li, J.R. Liu, S. Mahurin, J.H. Chen, D.K. Hensley, et al., Aromatic polyimide/graphene composite organic cathodes for fast and sustainable lithium-ion batteries, *Chemsuschem* 11 (4) (2018) 763–772.
- [35] W. Ai, W. Zhou, Z. Du, C. Sun, J. Yang, Y. Chen, et al., Toward high energy organic cathodes for Li-ion batteries: a case study of vat dye/graphene composites, *Adv. Funct. Mater.* 27 (19) (2017), 1603603.
- [36] L. Zhang, F. Zhang, X. Yang, G. Long, Y. Wu, T. Zhang, et al., Porous 3D graphene-based bulk materials with exceptional high surface area and excellent conductivity for supercapacitors, *Sci. Rep.* 3 (2013), <https://doi.org/10.1038/srep01408>.
- [37] T. Zhang, F. Zhang, L. Zhang, Y. Lu, Y. Zhang, X. Yang, et al., High energy density Li-ion capacitor assembled with all graphene-based electrodes, *Carbon* 92 (2015) 106–118.
- [38] X. Yang, L. Zhang, F. Zhang, Y. Huang, Y. Chen, Sulfur-infiltrated graphene-based layered porous carbon cathodes for high-performance lithium-sulfur batteries, *ACS Nano* 8 (5) (2014) 5208–5215.
- [39] Y. Wu, N. Yi, L. Huang, T. Zhang, S. Fang, H. Chang, et al., Three-dimensionally bonded spongy graphene material with super compressive elasticity and near-zero Poisson's ratio, *Nat. Commun.* 6 (2015), <https://doi.org/10.1038/ncomms7141>.
- [40] X. Chen, Y. Wu, Z. Huang, X. Yang, W. Li, L.C. Yu, et al., $\text{C}_{10}\text{H}_4\text{O}_2\text{S}_2$ /graphene composite as a cathode material for sodium-ion batteries, *J. Mater. Chem.* 4 (47) (2016) 18409–18415.
- [41] A.L. Ramirez, B.C. Chan, D.T. de Lill, Benzo 1,2-b':4,5-b' dithio-phene-4,8-dione, *Acta Crystallogr. E. Rep.* E68 (2012) o1428–o1428.
- [42] A. Ahmad, H. Wu, Y. Guo, Q. Meng, Y. Meng, K. Lu, et al., A graphene supported polyimide nanocomposite as a high performance organic cathode material for lithium ion batteries, *RSC Adv.* 6 (40) (2016) 33287–33294.
- [43] Y. Song, Y. Hu, Y. Sha, H. Rong, H. Wen, H.-J. Liu, et al., Graphene oxide linked with N, N-diamino-1,4,5,8-naphthalenetetracarboxylic bisimide as a stable cathode material for lithium-ion batteries, *Ionics* 25 (7) (2019) 2987–2995.
- [44] L. Zhao, W. Wang, A. Wang, Z. Yu, S. Chen, Y. Yang, A MC/AQ parasitic composite as cathode material for lithium battery, *J. Electrochem. Soc.* 158 (9) (2011) A991–A996.
- [45] F. Zhang, X. Yang, Y. Xie, N. Yi, Y. Huang, Y. Chen, Pyrolytic carbon-coated Si nanoparticles on elastic graphene framework as anode materials for high-performance lithium-ion batteries, *Carbon* 82 (2015) 161–167.